



**HAL**  
open science

## Analytical tether model for static kite flight

Nedeleg Bigi, Alain Nême, Kostia Roncin, Jean-Baptiste Leroux, Guilhem Bles, Christian Jochum, Yves Parlier

► **To cite this version:**

Nedeleg Bigi, Alain Nême, Kostia Roncin, Jean-Baptiste Leroux, Guilhem Bles, et al.. Analytical tether model for static kite flight. Roland Schmehl. Airborne Wind Energy: Advances in Technology Development and Research, Springer, pp.57-78, 2018, Green Energy and Technology, 978-981-10-1946-3. 10.1007/978-981-10-1947-0\_3 . hal-01804758

**HAL Id: hal-01804758**

**<https://ensta-bretagne.hal.science/hal-01804758>**

Submitted on 25 Jun 2021

**HAL** is a multi-disciplinary open access archive for the deposit and dissemination of scientific research documents, whether they are published or not. The documents may come from teaching and research institutions in France or abroad, or from public or private research centers.

L'archive ouverte pluridisciplinaire **HAL**, est destinée au dépôt et à la diffusion de documents scientifiques de niveau recherche, publiés ou non, émanant des établissements d'enseignement et de recherche français ou étrangers, des laboratoires publics ou privés.



Distributed under a Creative Commons Attribution 4.0 International License

# Analytical Tether Model for Static Kite Flight

Nedeleg Bigi, Alain Nême, Kostia Roncin, Jean-Baptiste Leroux, Guilhem Bles, Christian Jochum and Yves Parlier

**Abstract** The use of traction kites as auxiliary propulsion systems for ships appears to be a high-potential alternative for fuel saving. To study such a system a tether model based on the catenary curve has been developed. This model allows calculating static flight positions of the kite on the edge of the wind window. The effect of the wind velocity gradient is taken into account for the evaluation of the aerodynamic forces acting on kite and tether. A closed-form expression is derived for the minimum wind velocity required for static flight of the kite. Results are presented for a kite with a surface area of  $320 \text{ m}^2$  and a mass of  $300 \text{ kg}$  attached to a tether with a diameter of  $55 \text{ mm}$  and a mass per unit length of  $1.20 \text{ kg m}^{-1}$ . The minimum wind speed measured at  $10 \text{ m}$  altitude to launch the kite is found to be around  $4.5 \text{ m/s}$ . After the launching phase, we show that the optimal tether length for static flight is  $128.4 \text{ m}$  with a minimum wind speed of  $4.06 \text{ m/s}$ . The presented approach shows an error up to  $9\%$  for a zero-mass kite model with a straight massless tether regarding the maximal propulsion force estimation.

## 3.1 Introduction

This study is part of the beyond the sea<sup>®</sup> research program led by the ENSTA Bretagne school of engineering. The project attempts to develop a kite system as an auxiliary propulsion device for merchant ships. Such a system is a high-potential alternative to conventional fossil fuel based propulsion systems, as indicated by

---

Nedeleg Bigi (✉) · Alain Nême · Kostia Roncin · Jean-Baptiste Leroux · Guilhem Bles · Christian Jochum

ENSTA Bretagne, FRE CNRS 3744, IRDL, 29200 Brest, France

e-mail: nedeleg.bigi@ensta-bretagne.org

Y. Parlier

beyond the sea, 110 avenue de l'Europe, 33260 La Teste de Buch, France

e-mail: yves.parlier@beyond-the-sea.com

several authors [7, 17, 19, 23]. Depending on the maritime route and the seasons, weather conditions vary. Thus, to achieve a tether and a kite design according to the encountered weather condition, one of the main inputs of a functional specification is the minimum wind velocity enabling kite flight. The capacity of the system to tow a ship at a certain wind condition must be evaluated as well.

Moreover, wind speed increases with altitude, and as it has been highlighted by many authors, notably by Leloup et al. [17], this is a benefit for the kite to generate a propulsive force. This benefit is directly dependent on the tether length, the higher the kite is, the stronger the wind generally is. Therefore, during the early design stage, studies taking into account tether effects have to be performed. At this stage of the design a wide range of potential solutions must be investigated. This work aims therefore to provide an early design step accurate enough to be realistic.

Tethers are currently made of fiber materials such as Dyneema<sup>®</sup>(Ultra-high-molecular-weight polyethylene, UHMWPE) for example. This means that compression, transverse shear, bending and torsional stiffness of the tether can be neglected compared to its tensile stiffness. In addition, the tether shape is highly dependent on aerodynamic loading acting on the tether surface and tether gravity acting on the tether volume. This kind of structure has been studied for other industrial applications such as electrical power lines, anchored offshore structures, tethered underwater vehicles or sling loads. Tether models for airborne wind energy applications were inspired by these fields.

Williams et al. [24] developed a so-called lumped mass model for dynamic flight. The mass of each element is concentrated on each node and the distance between each node remains constant. Breukels and Ockels [4] used discrete element modeling with inelastic bar elements. Argatov et al. [1] accounted for tether sag due to wind load and gravity, assuming that the tension along the tether is constant. They proposed a method to calculate wind load by neglecting the tangential wind component relatively to the line. They showed how tether effects decrease the power production for a dynamic flight. A model considering the tether as a straight elastic spring to account for material stiffness has been used to study the stability of the kite during a dynamic flight by Terink et al. [21]. To identify the low wind limit for kite flight, the most restrictive flight case is assumed to be the static flight because the apparent wind velocity is, most of the time, lower compared to a dynamic flight.

Kite deployment and recovering phases can also reasonably be considered quasi-static. Indeed, with a constant reeling velocity and neglecting the dynamic effect on the tether, the kite follows a straight path at a constant speed, thus the kite flight can be considered as equivalent to a static flight. Moreover, Leloup et al. [17] have shown for upwind sailing that a static flight could be more efficient than dynamic flight for fuel saving. All these tether models have been developed for dynamic flight and are still valid for static flight. Nevertheless, for discrete model, artificial structural damping needs to be added to reach static equilibrium as reported by Breukels and Ockels [4]. Considering low wind velocities, tether sag could be important, therefore a single straight elastic spring modeling the tether [21] is not a realistic enough assumption. Varma and Goela [22] developed a soft kite tether model for static kite flights at zero azimuth angle. Their model is based on the catenary curve

[18]. Varma and Goela [22] consider a flexible tether of constant length and mass per unit length. Indeed, the average aerodynamic loading on the tether is not significantly modified by the increasing length of the tether due to its tensile stiffness.

Hobbs [10] studied the influence of the wind velocity gradient effect on the tether shape for static kite flights at zero azimuth angle. He concluded his study on the wind profile influence arguing that the main factor influencing the line shape is the mean wind velocity according to the altitude. Being analytical, the model presented by Varma and Goela [22] has the potential to sufficiently reduce computation times to perform tether analysis early in the design.

The study presented in this chapter provides an analytical formulation of the catenary curve [18, 22] to model a flexible tether of constant length for any static kite flight position, with an arbitrary attachment point altitude on the ship deck, and with a wind velocity gradient law for kite forces estimation. The preliminary content of the present chapter has been presented at the Airborne Wind Energy Conference 2015 [3]. The determination of tether's shape and tension only requires the solution of a one-dimensional transcendental equation with a fixed-point algorithm. This procedure improves the reliability and the convergence rate of 2D Newton's method suggested in [14]. A closed-form expression is determined to evaluate a mean aerodynamic loading on the tether according to the wind velocity gradient effect. These developments are then used to identify a new analytical low wind speed limit for kite flight. Then, results highlighting the capability of the model for an early design stage are presented.

## 3.2 Mathematical Model

### 3.2.1 Tether Model

The tether model is based on the well-known catenary curve [18]. As illustrated in Fig. 3.1, the points  $\mathbf{S}$  and  $\mathbf{K}$  mark the extremities of the tether namely the ship attachment point and the position of the kite. A constant load per unit length is applied on the tether, which is assumed to be flexible, of constant length and with no transverse shear and no bending stiffness. Consequently, the tether remains in a plane defined by  $(\mathbf{S}, \mathbf{y}_t, \mathbf{z}_t)$  of the  $R_t$  coordinate system.  $R_0 = (\mathbf{x}_0, \mathbf{y}_0, \mathbf{z}_0)$  denotes a coordinate system attached to the ship sailing at constant speed on a straight course, where  $\mathbf{z}_0$  is opposed to the earth gravity. The unit vector  $\mathbf{z}_t$  is defined by the load per unit length  $\mathbf{q}$  as

$$\mathbf{q} = -\|\mathbf{q}\|\mathbf{z}_t = -q\mathbf{z}_t. \quad (3.1)$$

The unit vector  $\mathbf{x}_t$  is defined as  $\mathbf{x}_t = (\mathbf{SK} \times \mathbf{z}_k) / \|\mathbf{SK} \times \mathbf{z}_k\|$ , where " $\times$ " denotes the cross product operator. In order to obtain a direct orthonormal coordinate system, the unit vector  $\mathbf{y}_t$  is given by  $\mathbf{y}_t = \mathbf{z}_t \times \mathbf{x}_t$ .

With tension  $\mathbf{T}$  along the tether,  $s$  the curvilinear abscissa,  $T_{y_t}$  and  $T_{z_t}$  denoting the projections  $\mathbf{T} \cdot \mathbf{y}_t$  and  $\mathbf{T} \cdot \mathbf{z}_t$ , the following equations define the static equilibrium

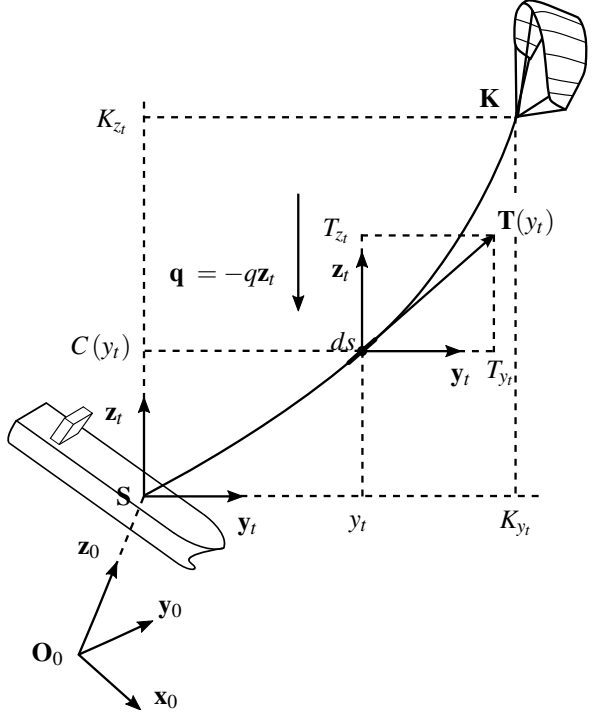


**Fig. 3.1** Coordinate systems used for the development of the catenary equation

of an infinitesimal length of tether  $ds$  projected on  $y_t$  and  $z_t$

$$\frac{dT_{y_t}}{ds} = 0, \quad (3.2)$$

$$\frac{dT_{z_t}}{ds} - q = 0. \quad (3.3)$$

According to Eqs. (3.2) and (3.3), a catenary function  $C$  must fulfill the following equation

$$\frac{q}{T_{y_t}} = \frac{C''(y_t)}{\sqrt{1 + C'(y_t)^2}}, \quad (3.4)$$

where  $C'$  and  $C''$  denote the first and second derivative of the function. Therefore, by integration of Eq. (3.4),  $C$  could be expressed as follows

$$C(y_t) = \frac{T_{y_t}}{q} \cosh\left(\frac{q}{T_{y_t}}y_t + K_1\right) + K_2, \quad (3.5)$$

where  $K_1$  and  $K_2$  are two constants of integration. They are determined with the boundary conditions

$$0 = \frac{T_{y_t}}{q} \cosh(K_1) + K_2, \quad (3.6)$$

$$K_{z_t} = \frac{T_{y_t}}{q} \cosh\left(\frac{q}{T_{y_t}} K_{y_t} + K_1\right) + K_2, \quad (3.7)$$

$$l_t = \int_0^{K_{y_t}} \sqrt{1 + C'^2(y_t)} dy_t, \quad (3.8)$$

$$= \frac{T_{y_t}}{q} \left[ \sinh\left(\frac{q}{T_{y_t}} K_{y_t} + K_1\right) - \sinh(K_1) \right], \quad (3.9)$$

where Eq. (3.9) is derived from constant tether length  $l_t$ , Eq. (3.6) from the coordinates of  $\mathbf{S} = [0, 0, 0]_{R_t}^\top$  and Eq. (3.7) from  $\mathbf{K} = [0, K_{y_t}, K_{z_t}]_{R_t}^\top$ . Using trigonometric identities, constants  $K_1$  and  $K_2$  can be expressed thanks to the boundary conditions in order to obtain the function  $C$  which can be expressed as

$$C(y_t) = \frac{K_{z_t} \sinh(\omega y_t) + \lambda \{ \sinh(\omega y_t) - \sinh(\omega K_{y_t}) + \sinh[\omega(K_{y_t} - y_t)] \}}{\sinh(\omega K_{y_t})}, \quad (3.10)$$

where  $\lambda$  and  $\omega$  are defined by

$$\lambda = \frac{l_t \sinh(\omega K_{y_t}) - K_{z_t} [\cosh(\omega K_{y_t}) - 1]}{2 [\cosh(\omega K_{y_t}) - 1]}, \quad (3.11)$$

$$\omega^2 (K_{z_t}^2 - l_t^2) = 2 [1 - \cosh(\omega K_{y_t})]. \quad (3.12)$$

It can be noticed that the catenary function does not depend on the load per unit length,  $q$ . Equation (3.12) can be rearranged in order to compute the value of  $\omega$ . With  $u = \omega^2 K_{y_t}^2$ ,  $\bar{l}_t = \frac{l_t}{K_{y_t}}$  and  $\beta = \frac{K_{z_t}}{K_{y_t}}$  we arrive at

$$u = \left\{ \operatorname{argcosh} \left[ \frac{u (\bar{l}_t^2 - \beta^2)}{2} + 1 \right] \right\}^2. \quad (3.13)$$

The value of  $u$  is computed by applying the fixed-point algorithm to Eq. (3.13) achieving convergence for all positive values of  $u$ . Thus, for a given kite position  $\mathbf{K}$  and a given ship attachment point position  $\mathbf{S}$ , tether tension is expressed by

$$\mathbf{T}(y_t) = \left[ 0, \frac{q}{\omega}, \frac{q}{\omega} C'(y_t) \right]_{R_t}^\top. \quad (3.14)$$

It can be noticed that the inverse of  $\omega$  is directly proportional to the tension in the  $y_t$  direction with the factor  $q$ . Consequently, tether shape and tension along the tether are determined for any kite and ship attachment point positions.

By contrast to the previous approach, an expression giving the kite location  $\mathbf{K}$ , for a known tension at  $\mathbf{K}$ , is relevant in order to determine the minimal wind velocity permitting a static flight. This expression is then developed. The tension is tangential to the tether, which means at  $\mathbf{K}$

$$C'(K_{y_t}) = \sinh\left(\frac{q}{T_{y_t}}K_{y_t} + K_1\right) = \frac{T_{z_t}}{T_{y_t}}. \quad (3.15)$$

Then, using Eqs. (3.6), (3.7) and (3.9), expressions for the kite location  $\mathbf{K}$  with a given tether tension at  $\mathbf{K}$  are

$$K_{y_t} = \frac{T_{y_t}}{q} \left[ \operatorname{argsinh}\left(\frac{T_{z_t}}{T_{y_t}}\right) - \operatorname{argsinh}\left(\frac{T_{z_t} - ql_t}{T_{y_t}}\right) \right], \quad (3.16)$$

$$K_{z_t} = \frac{T_{y_t}}{q} \left( \sqrt{1 + \left(\frac{T_{z_t}}{T_{y_t}}\right)^2} - \sqrt{1 + \left(\frac{T_{z_t} - ql_t}{T_{y_t}}\right)^2} \right). \quad (3.17)$$

Equations (3.16) and (3.17) are similar to [14, Eqs. (1.27) and (1.28)] in case of an flexible tether of constant length with very large Young's modulus.

### 3.2.2 Wind Model

It has been observed that the wind above the sea increases with the altitude due to the friction stress on the free surface within the atmospheric boundary layer. This phenomenon, called wind velocity gradient effect, can be taken into account with a simple formula according to ITTC [12]. The true wind velocity  $\mathbf{V}_{TW}$  at a given altitude  $z_0$  is calculated as

$$\mathbf{V}_{TW} = \mathbf{U}_{ref} \left( \frac{z_0}{z_{ref}} \right)^n, \quad (3.18)$$

from the known reference wind velocity  $\mathbf{U}_{ref}$  measured at an altitude  $z_{ref}$ . The coefficient  $n$  denotes the friction effect due to the free surface. A typical value of  $n = 1/7$  is given by ITTC [12] for sea friction. Figure 3.2 illustrates the evolution of the wind

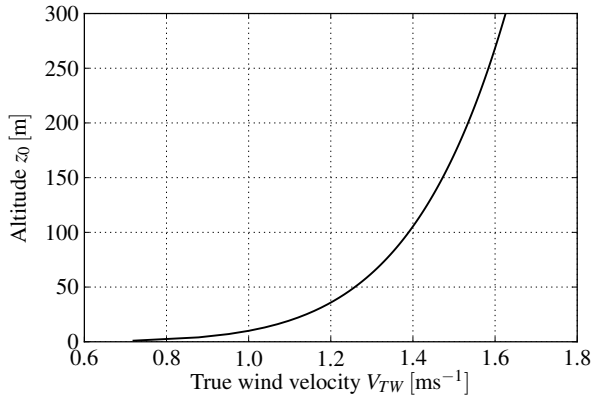


**Fig. 3.2** Wind velocity gradient evolution against altitude according to Eq. (3.18) using  $z_{ref} = 10$  m,  $U_{ref} = 1$  m s<sup>-1</sup> and  $n = 1/7$

velocity with the altitude range from 1 m to 300 m with a wind of  $1 \text{ m s}^{-1}$  at the reference altitude  $z_{ref} = 10 \text{ m}$ .

Consequently, since the relative wind velocity  $\mathbf{V}_{RW}$  is given by the difference between the true wind velocity and the ship velocity  $\mathbf{V}_s$ ,  $\mathbf{V}_{RW}$  can be expressed as

$$\mathbf{V}_{RW} = \mathbf{U}_{ref} \left( \frac{z_0}{z_{ref}} \right)^n - \mathbf{V}_s. \quad (3.19)$$

### 3.2.3 Tether Load Model

The load per unit length on the tether is given by

$$\mathbf{q}(s) = \mathbf{q}_w(s) + \mathbf{q}_g = \mathbf{q}_w(s) - m_t g \mathbf{z}_0, \quad (3.20)$$

where  $\mathbf{q}_w$  denotes the load per unit length due to wind and  $\mathbf{q}_g$  denotes weight distribution, along the curvilinear abscissa,  $m_t$  the mass per unit length of tether and  $g$  the acceleration due to gravity ( $g = 9.81 \text{ m s}^{-2}$ ).

Aerodynamic tether loading  $q_w$  is very sensitive since a tether can encounter a wide range of Reynolds number. The flow around circular cylinder has been widely studied in the past and is still a research topic as demonstrated by Sarpkaya in his literature review [20] and in Chap. 2 of this book. In addition, a textile rope has not exactly a circular section. Jung [15] performed wind tunnel experiments for various rope sections and various roughness surface at a Reynolds number  $Re = 84.0 \times 10^3$ . According to his measurements the drag coefficient can vary from 0.76 to 1.56 with orthogonal flow.

Nevertheless, since the Reynolds effect and the surface roughness are out of the scope of the paper, the Hoerner formulation [11] is used similar to many other authors involved in airborne wind energy. As mentioned in Sect. 3.2.2,  $\mathbf{V}_{RW}$  depends on altitude, and therefore  $\mathbf{q}_w$  as well. Since the catenary tether model requires only constant load per unit length, as can be seen in Sect.3.2.1, an approximation of constant wind tether load must be achieved. The determination of an equivalent altitude  $z_{q_0}$  to evaluate  $\mathbf{q}_w$  is proposed here. It is assumed that the tether is a straight line between  $\mathbf{S}$  and  $\tilde{\mathbf{K}}$ .  $\tilde{\mathbf{K}}$  is the kite position calculated with the static flight model described in [17] and summarized in Sect.3.2.5.

As illustrated in Fig. 3.3, the wind load  $\mathbf{q}_w$  can be decomposed into drag force  $\mathbf{q}_d$  and lift force  $\mathbf{q}_l$

$$\mathbf{q}_w = \mathbf{q}_l + \mathbf{q}_d. \quad (3.21)$$

Both components are determined from the Hoerner formulas [11] as



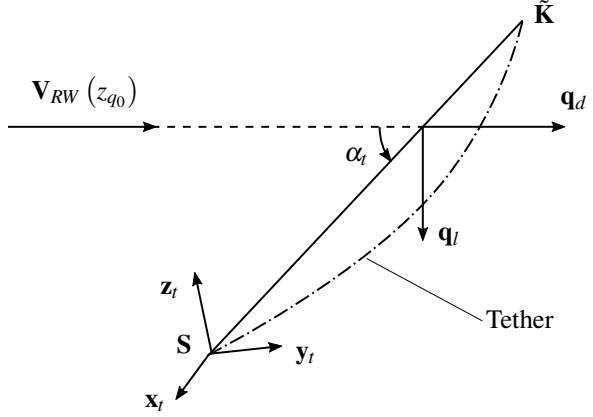


**Fig. 3.3** Diagram of the tether wind load model

$$\mathbf{q}_d = \frac{1}{2} \rho_a d_t [1.1 \sin^3(\alpha_t) + 0.02] \|\mathbf{V}_{RW}(z_{q_0})\| \mathbf{V}_{RW}(z_{q_0}), \quad (3.22)$$

$$\mathbf{q}_l = \frac{1}{2} \rho_a d_t [1.1 \sin^2(\alpha_t) \cos(\alpha_t)] \|\mathbf{V}_{RW}(z_{q_0})\| \frac{\mathbf{V}_{RW}(z_{q_0}) \times [\mathbf{V}_{RW}(z_{q_0}) \times \mathbf{S}\tilde{\mathbf{K}}]}{\|\mathbf{V}_{RW}(z_{q_0}) \times \mathbf{S}\tilde{\mathbf{K}}\|} \quad (3.23)$$

where  $\rho_a$  is the air density,  $d_t$  is the tether diameter,  $\alpha_t$  is the angle of attack between the wind and the tether as described in Fig. 3.3 and assuming a base drag coefficient of 1.1 for orthogonal flows ( $\alpha_t = \pi/2$ ).

With respect to the ship velocity  $\mathbf{V}_S$  and according to Eq. (3.18), the relative wind velocity at the altitude  $z_{q_0}$  is given by

$$\mathbf{V}_{RW}(z_{q_0}) = \mathbf{U}_{ref} \left( \frac{z_{q_0}}{z_{ref}} \right)^n - \mathbf{V}_S. \quad (3.24)$$

In order to conserve approximately the total force acting on the tether,  $z_{q_0}$  is defined such that the following equation must be fulfilled

$$\|\mathbf{V}_{RW}(z_{q_0})\|^2 = \frac{1}{(K_{z_0} - S_{z_0})} \int_{S_{z_0}}^{K_{z_0}} \|\mathbf{V}_{RW}(z)\|^2 dz, \quad (3.25)$$

which, by keeping only the largest root, leads to a second degree polynomial equation in  $z_{q_0}^n$

$$0 = \frac{\|\mathbf{U}_{ref}\|^2}{z_{ref}^{2n}} z_{q0}^{2n} - 2 \frac{\mathbf{V}_s \cdot \mathbf{U}_{ref}}{z_{ref}^n} z_{q0}^n + \|\mathbf{V}_s\|^2 - \|\mathbf{U}_{ref}\|^2 \frac{K_{z_0}^{2n+1} - S_{z_0}^{2n+1}}{(2n+1)(K_{z_0} - S_{z_0}) z_{ref}^{2n}} + 2 \mathbf{V}_s \cdot \mathbf{U}_{ref} \frac{K_{z_0}^{n+1} - S_{z_0}^{n+1}}{(n+1)(K_{z_0} - S_{z_0}) z_{ref}^n} - \|\mathbf{V}_s\|^2 \quad (3.26)$$

It must be noticed that the definition of the equivalent altitude  $z_{q0}$ , Eq. (3.25) is not correct to conserve the total force acting on the tether. Indeed, the load direction varies with the altitude which is not considered in Eq. (3.25). A better definition could have been

$$\mathbf{V}_{RW}(z_{q0}) = \frac{\mathbf{V}_2}{\sqrt{\|\mathbf{V}_2\|}}, \quad (3.27)$$

with,

$$\mathbf{V}_2 = \frac{1}{K_{z_0} - S_{z_0}} \int_{S_{z_0}}^{K_{z_0}} \|\mathbf{V}_{RW}\| \mathbf{V}_{RW} dz. \quad (3.28)$$

However, our proposition should be reasonable in order to achieve a closed-form formulation of the equivalent altitude  $z_{q0}$ .

### 3.2.4 Aerodynamic Kite Model

For a static flight, forces acting on the kite must be opposed to the tether tension and vary with altitude due to the wind velocity gradient. Applying the first Newton's law to the kite we obtain

$$0 = -\mathbf{T}(K_{y_t}) + \mathbf{L} + \mathbf{D} + \mathbf{W}, \quad (3.29)$$

where  $\mathbf{T}(K_{y_t})$  is the tether tension at kite location,  $\mathbf{L}$  is the lift kite aerodynamic force,  $\mathbf{D}$  is the drag kite aerodynamic force and  $\mathbf{W} = -M_K g \mathbf{z}_0$  is the kite weight calculated from the kite mass  $M_K$ . For static flight, the lift-to-drag ratio angle  $\varepsilon$  is assumed to be constant.  $\mathbf{D}$  is by definition in the direction of the relative wind and can be determined as follows

$$\mathbf{D} = \frac{1}{2} \rho_a A_K C_{L_K} \tan(\varepsilon) \|\mathbf{V}_{RW}\| \mathbf{V}_{RW}, \quad (3.30)$$

where  $\rho_a$  is the air density,  $A_K$  is the kite area and  $C_{L_K}$  is the kite lift coefficient. According to the assumption of a constant lift-to-drag ratio, the magnitude of the lift can be determined as

$$\|\mathbf{L}\| = \frac{\|\mathbf{D}\|}{\tan(\varepsilon)} \quad (3.31)$$

and the orthogonality of lift and drag components is formally expressed as

$$\mathbf{L} \cdot \mathbf{D} = 0. \quad (3.32)$$

One additional equation is needed to determine the lift. As a balance is expected between kite forces and tether tension, we know that at least they must stay in the plane  $(\mathbf{S}, \mathbf{y}_t, \mathbf{z}_t)$ . This is a consequence of the projection of Eq. (3.29) on axis  $\mathbf{x}_t$ , which can be expressed as

$$(\mathbf{L} + \mathbf{D} + \mathbf{W}) \cdot \mathbf{x}_t = 0. \quad (3.33)$$

The component  $L_{x_t}$  can be derived from Eq. (3.33) as

$$L_{x_t} = -(D_{x_t} + W_{x_t}). \quad (3.34)$$

Equations (3.31) and (3.32) lead to a second order polynomial equation in  $L_{z_t}$

$$L_{z_t} = \frac{\sqrt{\Delta} - L_{x_t} D_{x_t} D_{z_t}}{(D_{z_t}^2 + D_{y_t}^2)}, \quad \text{with} \quad (3.35)$$

$$\Delta = \frac{D_{y_t}^2 \|\mathbf{D}\|}{\tan^2(\varepsilon)} [D_{y_t}^2 + D_{z_t}^2 - L_{x_t}^2 \tan^2(\varepsilon)]. \quad (3.36)$$

Equation (3.36) describes the discriminant  $\Delta$  of the second order polynomial equation in  $L_{z_t}$ . Using Eq. (3.32)  $L_{y_t}$  can be derived as

$$L_{y_t} = -\frac{L_{x_t} D_{x_t} + L_{z_t} D_{z_t}}{D_{y_t}} \quad (3.37)$$

The condition  $\Delta \geq 0$  is a necessary condition to allow a static kite flight.

### 3.2.5 Zero-Mass Model

In this study, the zero-mass model developed by Leloup et al. [17] is used as reference model. This model has been expressed for static and dynamic kite flight. For a commodity purpose the corresponding static flight formulation is recalled with the present coordinate system. Neglecting the kite mass and the tether mass, the first Newton's law applied to the kite can be expressed by the following equation

$$\mathbf{0} = -\mathbf{T} + \mathbf{L} + \mathbf{D}, \quad (3.38)$$

where  $\mathbf{T}$  is given according to Leloup et al. [17] as

$$\mathbf{T} = \frac{\frac{1}{2} \rho_a A_k C_{Lk} \|\mathbf{V}_{RW}\|^2 \mathbf{SK}}{\cos(\varepsilon) \|\mathbf{SK}\|}. \quad (3.39)$$

We define the reference frame  $R_{RW} = (\mathbf{S}, \mathbf{x}_{RW}, \mathbf{y}_{RW}, \mathbf{z}_0)$ , with  $\mathbf{x}_{RW} = \mathbf{V}_{RW} / \|\mathbf{V}_{RW}\|$  and  $\mathbf{y}_{RW} = \mathbf{z}_0 \times \mathbf{x}_{RW}$ , as illustrated in Fig. 3.4, to obtain

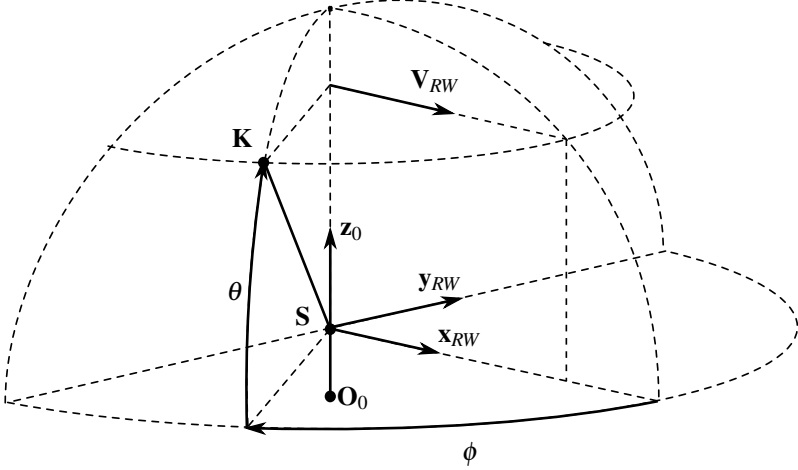


**Fig. 3.4** Zero-mass model parametrization of Leloup et al. [17]. In this diagram, the azimuth angle  $\phi$  is negative

$$\mathbf{SK} = [l_t \cos(\phi) \cos(\theta), l_t \sin(\phi) \cos(\theta), l_t \sin(\theta)]_{R_{RW}}^{\top}. \quad (3.40)$$

The static flight condition is calculated by Leloup et al. [17] as

$$\phi = \pm \arccos \left[ \frac{\sin(\varepsilon)}{\cos(\theta)} \right] \quad (3.41)$$

### 3.2.6 Kite Static Equilibrium

The equilibrium equation of the kite, Eq. (3.29), can be solved by coupling these models. The initial kite position is determined according to the zero-mass formulation of the kite balanced equation, as shown in Sect. 3.2.5. From this position, the tether load and coordinate system  $R_t$  are calculated, as shown in Sect. 3.2.1, and kept constant until the kite equilibrium position is reached. A Newton-Raphson algorithm, in Eq. (3.42), is used to solve the kite static equilibrium in plane  $(\mathbf{y}_t, \mathbf{z}_t)$

$$\begin{bmatrix} K_{y_t} \\ K_{z_t} \end{bmatrix}_{(k+1)} = \begin{bmatrix} K_{y_t} \\ K_{z_t} \end{bmatrix}_{(k)} - \begin{bmatrix} \frac{\partial F_{y_t}}{\partial K_{y_t}} & \frac{\partial F_{y_t}}{\partial K_{z_t}} \\ \frac{\partial F_{z_t}}{\partial K_{y_t}} & \frac{\partial F_{z_t}}{\partial K_{z_t}} \end{bmatrix}_{(k)}^{-1} \begin{bmatrix} F_{y_t} \\ F_{z_t} \end{bmatrix}_{(k)}, \quad (3.42)$$

where  $\mathbf{F} = -\mathbf{T} + \mathbf{L} + \mathbf{D} + \mathbf{W}$  and  $k$  represents the iteration number.

### 3.2.7 Verification of the Implementation

The implementation of the presented model is verified on the basis of the experimental data of Irvine and Sinclair in [13]. In this experiment, the two extremities of a cable were horizontally attached. The cable length was 1.20 m, the cable cross sectional area was  $1.58 \cdot 10^{-6} \text{ m}^2$  and the Young's modulus of the cable was  $1.00 \times 10^{11} \text{ N m}^{-2}$ . The horizontal distance between the attachment point was 1.00 m. A total of 20 weights of 2.45 N were added to the cable with ferrules in order to neglect the cable bending stiffness. From the attachment point, the weights were attached with a distance of 0.03 m and the weights were equally spaced each other by a distance of 0.06 m. The weight of the cable, ferrules and weights were 50 N. Figure 3.5 represents the cable corresponding to the experiment in [13] (dashed line) and the corresponding cable shape calculated with model, Eqs. (3.10) – (3.13). The experimentally measured shape of the cable has been extracted from [13].

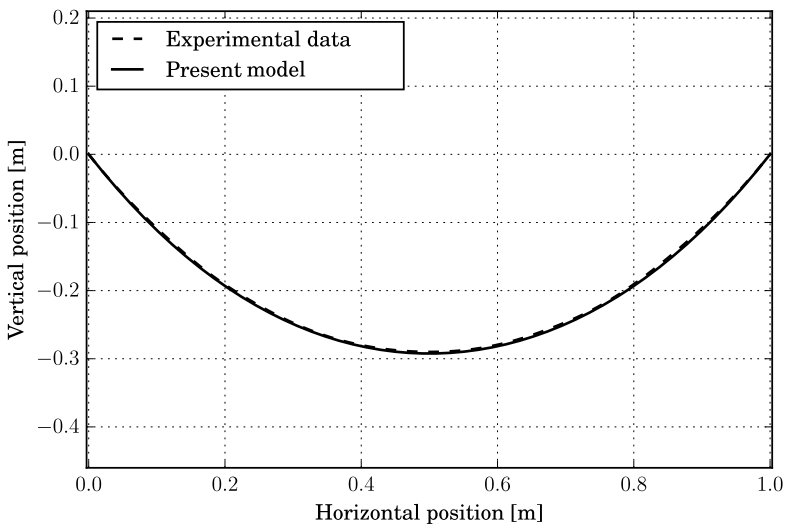


**Fig. 3.5** Comparison of the tether shape computed with the present model and measured by [13]

The present model fits pretty well with the experimental data [13] and can be considered validated. Nevertheless, a comparison between the entire present model and static kite flight must be investigated as well.

## 3.3 Low Wind Limit for Kite Flight

Most kite launch step begins by quasi-static flight at zero azimuth angle. Therefore the low wind limit for static kite flight at zero azimuth angle is an important param-

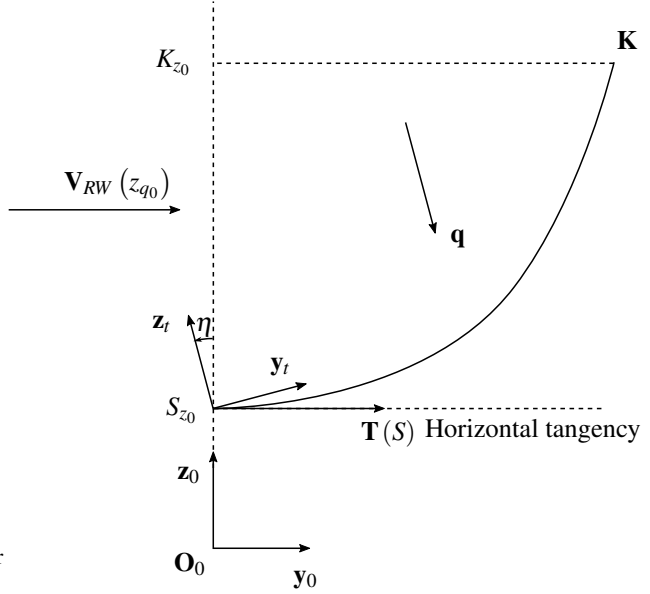


**Fig. 3.6** Diagram of the lower limit static flight case

eter. Obviously, a tether should not touch the ground or the free surface. In that case, friction with the ground could have a dramatic effect on the material durability and kite control. This leads to the mathematical condition that the whole tether must be above the attachment point, as shown in Fig. 3.6. The mathematical expression of this limit is given by

$$\mathbf{T}(S) \cdot \mathbf{z}_0 = 0. \quad (3.43)$$

In the static kite flight case at zero azimuth angle, the first Newton's law applied to the tether and projected on axis  $\mathbf{z}_0$ , in accordance with the condition given by Eq. (3.43), leads to

$$L - W + l_t \mathbf{q} \cdot \mathbf{z}_0 = 0. \quad (3.44)$$

Therefore, the relative wind at the kite location is given by

$$V_{RW} = \sqrt{\frac{2(W - l_t \mathbf{q} \cdot \mathbf{z}_0)}{\rho_a A_k C_{L_K}}}. \quad (3.45)$$

In the static kite flight at zero azimuth angle, the kite position in reference frame  $R_0$ , compared to the position in reference frame  $R_t$ , is defined by the angle

$$\eta = \arctan \left( -\frac{\mathbf{q} \cdot \mathbf{y}_0}{\mathbf{q} \cdot \mathbf{z}_0} \right). \quad (3.46)$$

Kite altitude in  $R_0$  is given by

$$K_{z_0} = S_{z_0} + K_{y_t} \sin(\eta) + K_{z_t} \cos(\eta). \quad (3.47)$$

Inserting Eqs. (3.45) and (3.47) into Eq. (3.24), assuming  $\mathbf{V}_{RW}$  and  $\mathbf{V}_s$  are collinear, and reorganizing leads to the wind velocity at the measurement altitude

$$U_{ref,min} = \frac{z_{ref}^n}{[S_{z_0} + K_{y_t} \sin(\eta) + K_{z_t} \cos(\eta)]^n} \left[ \sqrt{\frac{2(W - l_t \mathbf{q} \cdot \mathbf{z}_0)}{\rho_a A_k C_{Lk}}} + V_s \right]. \quad (3.48)$$

As indicated by Eqs. (3.20) – (3.24),  $\mathbf{q}$  depends on  $U_{ref,min}$  which means that Eq. (3.48) needs to be solved. However, rather than solving the problem numerically, for example by iterative methods, a closed-form approximation of the minimal wind velocity required for a static flight is provided assuming that the load per unit length on the tether is only due to the gravity (this hypothesis is discussed at the end of the Sect. 3.5 and is illustrated in Fig. 3.10). Therefore,  $\mathbf{z}_t$  is equal to  $\mathbf{z}_0$  and the load per unit length is  $\mathbf{q} = \mathbf{q}_g$ . Then, the closed-form Eq. (3.45) becomes

$$V_{RW} = \sqrt{\frac{2(W + m_t l_t g)}{\rho_a A_k C_{Lk}}}, \quad (3.49)$$

where  $g = 9.81 \text{ m s}^{-2}$  is the acceleration due to gravity. Using Eqs. (3.17) and (3.24), the lower limit is

$$U_{ref,min}^- = \frac{z_{ref}^n \left( \sqrt{\frac{2g(M_k + l_t m_t)}{\rho_a A_k C_{Lk}}} + V_s \right)}{\left\{ S_{z_0} + \tan(\varepsilon) \left( l_t + \frac{M_k}{m_t} \right) \left[ \sqrt{1 + \left( \frac{m_t l_t}{(m_t l_t + M_k) \tan(\varepsilon)} \right)^2} - 1 \right] \right\}^n}. \quad (3.50)$$

Using the following dimensionless problem parameters

$$\begin{aligned} \tilde{U} &= U_{ref,min}^- \sqrt{\frac{A_k \rho_a C_{Lk}}{2W}}, & \tilde{l}_t &= \frac{m_t l_t}{M_k}, & \tilde{S} &= \frac{S_{z_0}}{z_{ref}}, \\ \tilde{V}_s &= V_s \sqrt{\frac{A_k \rho_a C_{Lk}}{2W}}, & \tilde{z} &= \frac{z_{ref} m_t}{M_k}, \end{aligned}$$

Eq. (3.50) can be normalized to

$$\tilde{U} = \frac{\sqrt{1 + \tilde{l}_t + \tilde{V}_s}}{\left\{ \tan(\varepsilon) \frac{(1 + \tilde{l}_t)}{\tilde{z}} \left[ \sqrt{1 + \left[ \frac{\tilde{l}_t}{\tan(\varepsilon)(1 + \tilde{l}_t)} \right]^2} - 1 \right] + \tilde{S} \right\}^n}. \quad (3.51)$$

The parameter  $\tilde{l}_t$  can be interpreted as the dimensionless tether length. The attachment point altitude is normalized by the wind measurement altitude. The parameter  $\tilde{z}$  characterizes the tether mass per unit length compared to the kite mass. This last parameter provides information on the structural and material design priority be-

tween the tether and the kite, it increases when the ratio of safety factors between the line and the kite increases.

### 3.4 Case Study

The following example calculations are based on the case study of Dadd [5] where kite parameters have been extrapolated from data measured by Dadd et al. [6] for a Flexifoil<sup>®</sup> Blade III kite with 3 m<sup>2</sup> surface area. Kite and tether characteristics are summarized in Table 3.1. Tether diameter and mass per unit length have been estimated using a dynamic flight load case calculated with the analytical zero-mass model developed by Leloup et al. [17]. The flight trajectory is taken from Argatov et al. [2] with a polar angle amplitude of 16° and an azimuth angle amplitude of 66°. For a true wind speed of 17 m s<sup>-1</sup> and for a cruising ship speed of 7.5 m s<sup>-1</sup>, according to the model of Leloup et al. [17], maximum tether tension is given for a true wind angle<sup>1</sup> of 110°. At this configuration the tether tension is  $1.5 \times 10^6$  N.

**Table 3.1** Kite and tether characteristics for the study. Estimated values are marked by an asterisk (\*)

Flexifoil <sup>®</sup> Blade III characteristics extrapolated by [5]		
Wing surface area	$A_K$	320 m <sup>2</sup>
Wing mass*	$M_K$	300 kg
Aerodynamic lift coefficient	$C_L$	0.776 -
Lift-to-drag ratio angle	$\epsilon$	12.02 deg
Tether characteristics		
Length	$l_t$	300 m
Mass per unit length*	$m_t$	1.20 kg m <sup>-1</sup>
Diameter*	$d_t$	55.0 mm

The chosen material of the tether is Ultra-High Molecular Weight Polyethylene (UHMWPE), which is also known under the brand name Dyneema<sup>®</sup>. According to its ultimate specific stress [8, 9, 16] of  $1.46 \times 10^3$  J g<sup>-1</sup> and a safety factor of 1.2, a maximal load of  $1.25 \times 10^6$  N is allowed. This leads to a tether with a mass per unit length of 1.2 kg m<sup>-1</sup> and a diameter of 55 mm.

For the results presented in Sects. 3.5 and 3.6, the ship attachment point altitude  $S_{z_0}$  is 10 m and the true wind speed is measured at an altitude of  $z_{ref} = 10$  m. According to the ITTC [12], the wind velocity gradient parameter is  $n = 1/7$ .

<sup>1</sup> The true wind angle is the angle between the ship path and the true wind velocity at the reference altitude [17]



### 3.5 Minimal Wind Velocity

In order to identify a low wind limit for static kite flight, the criterion of Sect. 3.3 is applied with  $\varepsilon = 12.02^\circ$ . Figure 3.7 represents three surface plots of the non-dimensional minimal wind velocity  $\tilde{U}$  defined by Eq. (3.51) as a function of the non-dimensional parameters  $\tilde{z}$  and  $\tilde{l}_t$  for  $\tilde{V}_s = 0$  and for three specific values of  $\tilde{S}$ .

Assuming a given value of  $\tilde{l}_t$ , Fig.3.7 shows that the non-dimensional minimal wind velocity  $\tilde{U}$  increases when the ratio  $m_t l_t / M_K$  increases or when the ratio  $\tilde{S}$  increases. These results make sense in a natural way. The explanation of the variation of  $\tilde{U}$  according to the tether length is less obvious as it can be observed in Fig.3.7. An optimal tether length can appear to minimize  $\tilde{U}$ . Nevertheless the main result is that the non-dimensional minimal wind velocity increases when the tether length increases beyond a finite value which can be zero. This result is important for keeping the kite airborne. Finally the effective minimal wind velocity  $U_{ref,min}^-$  is obtained by dividing  $\tilde{U}$  by the factor  $\sqrt{A_k \rho_a C_{LK} / (2W)}$ . The latter increases when the kite weight to lift coefficient ratio increases.

For the investigated case described in Sect. 3.4 and a zero ship velocity, the minimal wind velocity  $U_{ref,min}^-$  given by Eq. (3.50) has been plotted in Fig. 3.8 for different tether lengths from 0 to 400 m. For a tether length  $l_t = 0$ , the minimal required wind speed is  $4.44 \text{ m s}^{-1}$ . Then, the minimal wind speed required increases to reach a maximum at  $4.48 \text{ m s}^{-1}$  for a tether length of 8 m. With longer tether, the minimal required wind speed decreases to  $4.06 \text{ m s}^{-1}$  for  $l_t = 128 \text{ m}$ . The third part

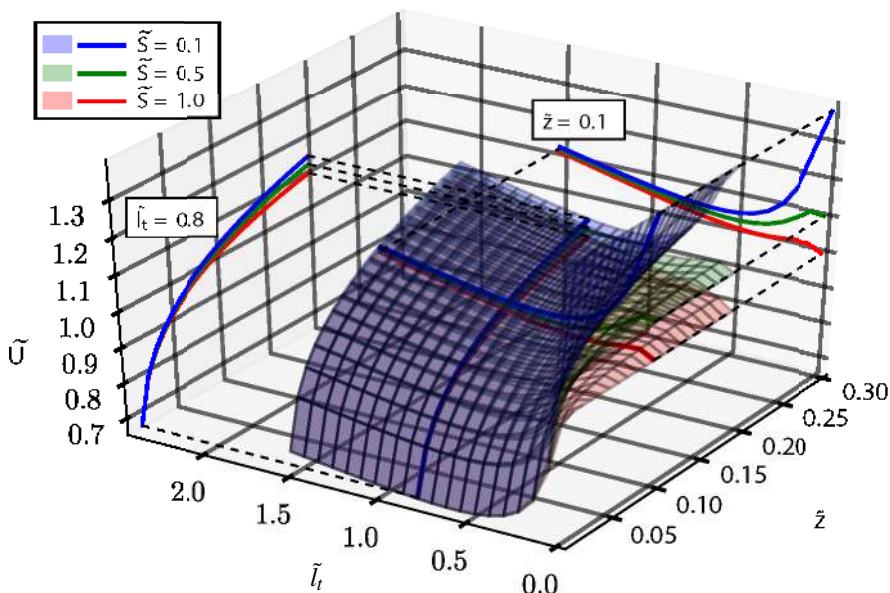


**Fig. 3.7** Surface plots of the non-dimensional minimum wind velocity  $\tilde{U}$  as function of the non-dimensional parameters  $\tilde{z}$  and  $\tilde{l}_t$  for  $\tilde{S} = 0.1, 0.5$  and  $1$

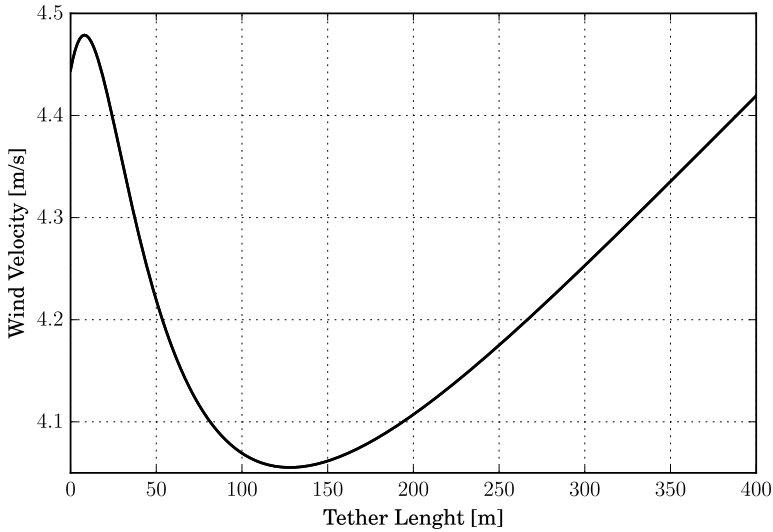


**Fig. 3.8** Minimal wind velocity  $U_{ref}$  at  $z_{ref} = 10$  m for a tether length  $l_t$  from 0 to 400 m

of the curve increases. A tether length of 128.4 m is optimal to allow a static flight for a minimal true wind speed. For this tether length the required true wind speed is  $4.06 \text{ m s}^{-1}$ .

On one hand, the longer the tether, the higher the kite is. So, due to the wind velocity gradient effect, the relative wind speed at the kite increases with the tether length. On the other hand, tether weight increases with tether length. In Fig. 3.8 it can be noticed that for tether length such as  $8 \leq l_t \leq 128$  m the increase of the relative wind speed is more significant than the increase of the tether weight  $m_t l_t$ . This has the effect of reducing the minimal wind speed required to allow a static flight. For tether length such as  $0 \leq l_t \leq 8$  m and  $l_t \geq 128$  m, the phenomenon is reversed. The increase of the wind speed is no longer sufficient to counteract the increase of the tether gravitational load.

Figure 3.9 shows the minimum wind required to allow a static flight for different lift-to-drag ratio angles  $\varepsilon = \arctan(D/L)$ . Here, for low range of  $\varepsilon$ , the wind velocity required increases linearly with  $\varepsilon$ .

In this section, the effect of gravity on the tether has been taken into account while the influence of the aerodynamic loading has been neglected. For a static flight case at zero azimuth angle and for a tether length of 300 m, a comparison between aerodynamic load and gravitational load on the tether is displayed in Fig. 3.10.

The diagram clearly shows that for the minimum wind speed of  $4.5 \text{ m s}^{-1}$ , which is required for static flight according to Fig. 3.8, the corresponding wind load is less than 12.5% of the gravitational load. Thereby, in order to obtain a closed-form for-

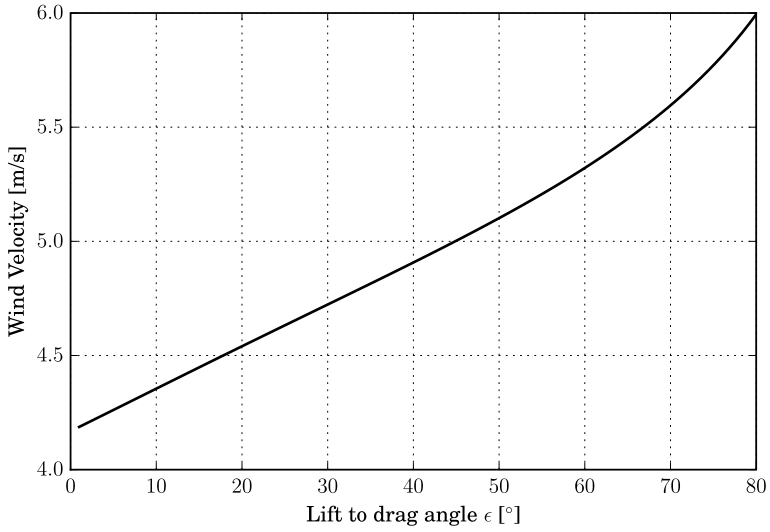


**Fig. 3.9** Minimal wind velocity  $U_{ref}$  at  $z_{ref} = 10$  m for a lift-to-drag angle  $\epsilon$  range from  $1^\circ$  to  $80^\circ$

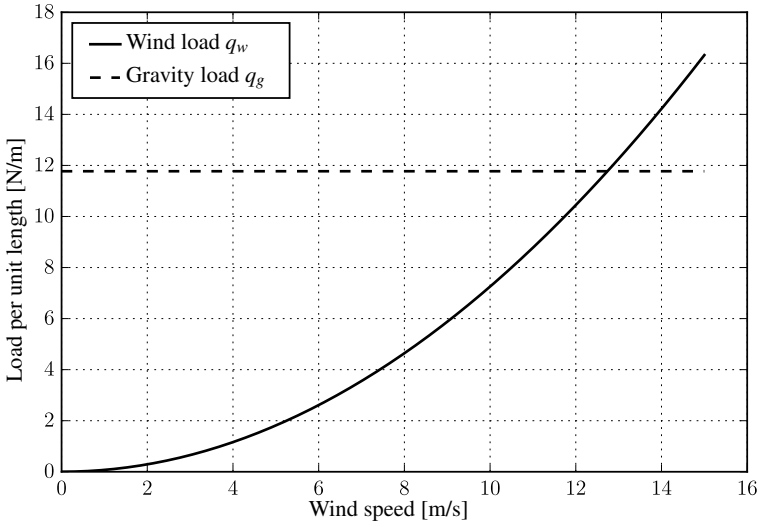


**Fig. 3.10** Tether load per unit length due to wind  $q_w$  and tether load per unit length due to gravity  $q_g$  for a wind  $U_{ref}$  range from  $0 \text{ m s}^{-1}$  to  $15 \text{ m s}^{-1}$  at  $z_{ref} = 10$  m

mula to determine the minimal wind speed to allow a static flight, the assumption of neglecting the aerodynamic force can be considered as being reasonable. However, it can be expected that within the framework of this hypothesis, the low wind speed limit is underestimated.

### 3.6 Tether Tension

Figure 3.11 represents tether tension for all azimuth angles enabling a static flight at wind condition  $\mathbf{U}_{ref} = [0, 7.5, 0]_{R_0}^\top \text{ m s}^{-1}$  and ship velocity  $\mathbf{V}_s = [7.5, 0, 0]_{R_0}^\top \text{ m s}^{-1}$ . Two models are compared. Solid and dashed lines are respectively the tension calculated with the present model at ship position  $\mathbf{S}$  and kite position  $\mathbf{K}$ . The dotted line represents static flight tension calculated with the model of [17]. Red, black and blue lines are the tension projected on the unit vector  $\mathbf{x}_0$ ,  $\mathbf{y}_0$  and  $\mathbf{z}_0$ , respectively.

For the presented model, a difference in tension between the ground and kite attachment points can be noticed. This difference is significant for the tensions projected on the axis  $\mathbf{z}_0$  and it is caused by the tether weight and aerodynamic loads but as well by the tension direction differences between  $\mathbf{S}$  and  $\mathbf{K}$ .

Leloup et al. [17] consider a straight tether and do not take into account tether loading and kite weight, leading therefore to no differences in tension between the kite and the attachment point. Moreover for a given azimuth, kite altitude is higher for the zero-mass model than for the present model. Combined with the wind veloc-

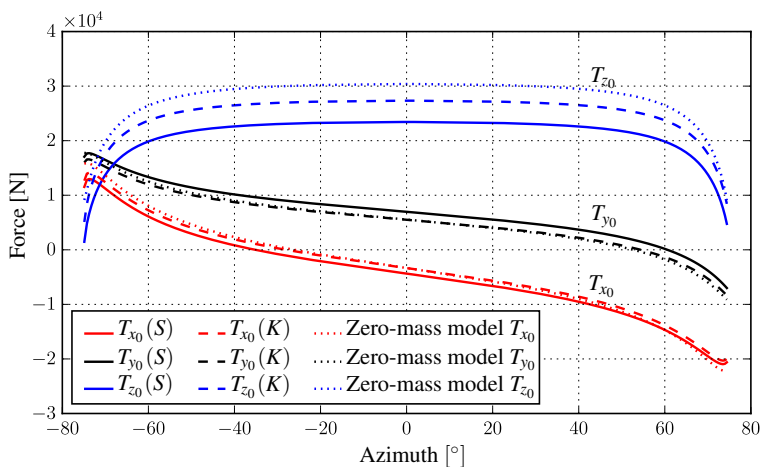


**Fig. 3.11** Tether forces projected in frame  $R_0$  for azimuth angle from  $-75^\circ$  to  $75^\circ$  calculated with the present model at ship attachment point  $\mathbf{S}$  and kite position  $\mathbf{K}$  and with the zero-mass model presented in Sect. 3.2.5

ity gradient effect, this leads to a higher kite aerodynamic force with the model of Leloup et al. [17].

The propulsive part of the tether tension is the tension projected along the ship path,  $T_{x_0}(\mathbf{S})$ . The optimal position of the kite to generate the maximum propulsive force is reached for an azimuth angle of  $-73.67^\circ$  for both models. We denote  $F_{P_0}$  as the propulsive force obtained with the zero-mass model of Leloup et al. [17]. At this azimuth angle the dimensionless difference between  $F_{P_0}$  and  $T_{x_0}(\mathbf{S})$ , defined by

$$\Delta_p = \frac{F_{P_0} - T_{x_0}(\mathbf{S})}{T_{x_0}(\mathbf{S})} \quad (3.52)$$

for a ship velocity  $\mathbf{V}_s = [7.5, 0, 0]_{R_0}^\top \text{ m s}^{-1}$  and for a wind velocity range from  $\mathbf{U}_{ref} = [0, 5, 0, 0]_{R_0}^\top \text{ m s}^{-1}$  to  $\mathbf{U}_{ref} = [0, 20, 0, 0]_{R_0}^\top \text{ m s}^{-1}$ , is plotted in Fig. 3.12. It can be

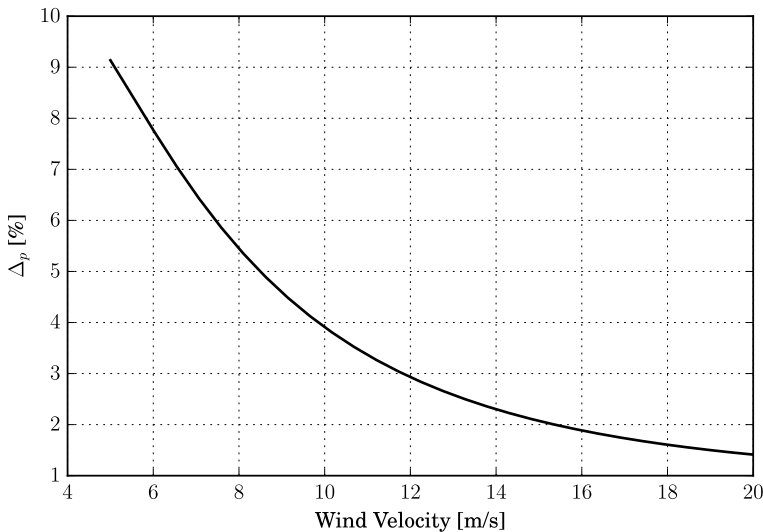


**Fig. 3.12** Plot of Eq. (3.52), the dimensionless difference of propulsion forces calculated with the present model compared to propulsion forces calculated with the zero-mass model described in Sect. 3.2.5 for a wind range from  $5 \text{ m s}^{-1}$  to  $20 \text{ m s}^{-1}$  at  $z_{ref} = 10 \text{ m}$

noticed from this diagram that the relative difference between  $F_{P_0}$  and  $T_{x_0}(\mathbf{S})$  is up to 9% for a wind speed of  $5 \text{ m s}^{-1}$  and decreases to almost 1.5% for a wind speed of  $20 \text{ m s}^{-1}$ . The error decreases with an increasing wind velocity because of tether loading. Kite weight and sag effects become smaller compared to the kite aerodynamic force. This shows that it is particularly important to take into account tether deformation due to tether loading at low wind speed. By contrast, at high-speed wind, the propulsive force error tends to 1%.

### 3.7 Conclusion

A three-dimensional analytical model for the tether deformation due to gravity and aerodynamic loading has been derived in this chapter. The effect of the wind velocity gradient has been taken into account both for the tether as well as for the kite aerodynamics. A method for determining a low wind speed limit for kite flight has been developed. This method allows for a comparative study between the influence of tether design, in terms of length and mass per unit length, and kite design, in terms of lift-to-drag ratio angle, lift coefficient and mass. For the present case study, an optimal tether length around 128 m has been identified in order to allow a static flight at a minimal wind velocity. A wind speed above  $4.5 \text{ m s}^{-1}$  is required to launch the kite. Finally, the presented model indicates an error up to 9% for the zero-mass kite model with a straight zero-mass tether on propulsion force estimation with a static kite flight case.

For this study a tether drag coefficient of 1.1 has been assumed. Jung [15] shows how coating can be used to effectively reduce the aerodynamic drag of the tether. Because a coated rope is heavier it should be analyzed whether the increased tether mass justifies the achievable drag reduction when considering the low wind limit for static kite flight. The presented model could be an interesting starting point to study these competing effects.

In addition, the solution for the static position of a kite in a wind field with velocity gradient is computed in less than 1 s on a common PC. Because of these short calculation times the model is suitable for coupled simulations of a ship towed by a kite for maneuvering and seakeeping assessments. The accuracy of the presented model will further be assessed by comparison with finite element simulations which is currently in progress.

### References

1. Argatov, I., Rautakorpi, P., Silvennoinen, R.: Apparent wind load effects on the tether of a kite power generator. *Journal of Wind Engineering and Industrial Aerodynamics* **99**(5), 1079–1088 (2011). doi: 10.1016/j.jweia.2011.07.010
2. Argatov, I., Rautakorpi, P., Silvennoinen, R.: Estimation of the mechanical energy output of the kite wind generator. *Renewable Energy* **34**(6), 1525–1532 (2009). doi: 10.1016/j.renene.2008.11.001
3. Bigi, N., Nême, A., Roncin, K., Leroux, J.-B., Bles, G., Jochum, C., Parlier, Y.: A Quasi-Analytical 3D Kite Tether Model. In: Schmehl, R. (ed.). *Book of Abstracts of the International Airborne Wind Energy Conference 2015*, p. 43, Delft, The Netherlands, 15–16 June 2015. doi: 10.4233/uuid:7df59b79-2c6b-4e30-bd58-8454f493bb09. Presentation video recording available from: <https://collegerama.tudelft.nl/Mediasite/Play/0ed3695b3d284dd190f5162cdc5b806a1d>
4. Breukels, J.: Kite launch using an aerostat. Technical Report, Delft University of Technology, 21 Aug 2007. <http://repository.tudelft.nl/view/ir/uuid%3A1a0c6dfd-6115-461f-ac04-bd8751efd6fb>

5. Dadd, G. M.: Kite dynamics for ship propulsion. Ph.D. Thesis, University of Southampton, 2013. <http://eprints.soton.ac.uk/id/eprint/351348>
6. Dadd, G. M., Hudson, D. A., Shenoï, R. A.: Determination of kite forces using three-dimensional flight trajectories for ship propulsion. *Renewable Energy* **36**(10), 2667–2678 (2011). doi: 10.1016/j.renene.2011.01.027
7. Duckworth, R.: The application of elevated sails (kites) for fuel saving auxiliary propulsion of commercial vessels. *Journal of Wind Engineering and Industrial Aerodynamics* **20**(1–3), 297–315 (1985). doi: 10.1016/0167-6105(85)90023-6
8. Fer, F.: *Thermodynamique macroscopique*, vol. 2. Gordon & Breach (1971)
9. Fitzgerald, J. E.: A tensorial Hencky measure of strain and strain rate for finite deformations. *Journal of Applied Physics* **51**(10), 5111–5115 (1980). doi: 10.1063/1.327428
10. Hobbs, S. E.: *A Quantitative Study of Kite Performance in Natural Wind with Application to Kite Anemometry*. Ph.D. Thesis, Cranfield University, 1986. <https://dspace.lib.cranfield.ac.uk/bitstream/1826/918/2/sehphd2a.pdf>
11. Hoerner, S. F.: *Fluid-Dynamic Drag*. Bricktown, Brick Town, NJ, USA (1965)
12. International Towing Tank Conference: ITTC Symbols and Terminology List Version 2014, Sept 2014. <http://ittc.info/media/4004/structured-list2014.pdf>
13. Irvine, H. M., Sinclair, G. B.: The suspended elastic cable under the action of concentrated vertical loads. *International Journal of Solids and Structures* **12**(4), 309–317 (1976). doi: 10.1016/0020-7683(76)90080-9
14. Irvine, H. M.: *Cable structures*. MIT Press, London (1981)
15. Jung, T. P.: Wind Tunnel Study of Drag of Various Rope Designs. AIAA Paper 2009-3608. In: *Proceedings of the 27th AIAA Applied Aerodynamics Conference*, San Antonio, TX, USA, 22–25 June 2009. doi: 10.2514/6.2009-3608
16. Leclère, G., Nème, A., Cognard, J., Berger, F.: Rupture simulation of 3D elastoplastic structures under dynamic loading. *Computers & Structures* **82**(23–26), 2049–2059 (2004). doi: 10.1016/j.compstruc.2004.03.073
17. Leloup, R., Roncin, K., Behrel, M., Bles, G., Leroux, J.-B., Jochum, C., Parlier, Y.: A continuous and analytical modeling for kites as auxiliary propulsion devoted to merchant ships, including fuel saving estimation. *Renewable Energy* **86**, 483–496 (2016). doi: 10.1016/j.renene.2015.08.036
18. Lewis, W. J.: *Tension Structures: Form and Behaviour*. Thomas Telford, London (2003)
19. Naaijen, P., Koster, V.: Performance of auxiliary wind propulsion for merchant ships using a kite. In: *Proceedings of the 2nd International Conference on Marine Research and Transportation*, pp. 45–53, Naples, Italy, 28–30 June 2007. <http://www.icmrt07.unina.it/Proceedings/Papers/c/26.pdf>
20. Sarpkaya, T.: A critical review of the intrinsic nature of vortex-induced vibrations. *Journal of Fluids and Structures* **19**(4), 389–447 (2004). doi: 10.1016/j.jfluidstructs.2004.02.005
21. Terink, E. J., Breukels, J., Schmehl, R., Ockels, W. J.: Flight Dynamics and Stability of a Tethered Inflatable Kiteplane. *AIAA Journal of Aircraft* **48**(2), 503–513 (2011). doi: 10.2514/1.C031108
22. Varma, S. K., Goela, J. S.: Effect of wind loading on the design of a kite tether. *Journal of Energy* **6**(5), 342–343 (1982). doi: 10.2514/3.48051
23. Wellicome, J. F.: Some comments on the relative merits of various wind propulsion devices. *Journal of Wind Engineering and Industrial Aerodynamics* **20**(1–3), 111–142 (1985). doi: 10.1016/0167-6105(85)90015-7
24. Williams, P., Lansdorp, B., Ockels, W. J.: Modeling and Control of a Kite on a Variable Length Flexible Inelastic Tether. AIAA Paper 2007-6705. In: *Proceedings of the AIAA Modeling and Simulation Technologies Conference and Exhibit*, Hilton Head, SC, USA, 20–23 Aug 2007. doi: 10.2514/6.2007-6705